

## Controlled Multistep Self-Assembling of Colloidal Droplets at a Nematic Liquid Crystal–Air Interface

Nan Wang,<sup>1</sup> Julian S. Evans,<sup>1,§</sup> Chenxi Li,<sup>1</sup> Victor M. Pergamenschchik,<sup>2,†</sup>  
Ivan I. Smalyukh,<sup>3,4,‡</sup> and Sailing He<sup>1,5,\*</sup>

<sup>1</sup>Centre for Optical and Electromagnetic Research, State Key Laboratory of Modern Optical Instrumentation, College of Optical Science and Engineering, Zhejiang University, Hangzhou 310058, China

<sup>2</sup>Department of Theoretical Physics, Institute of Physics, prospect Nauki, 46, Kiev 03039, Ukraine

<sup>3</sup>Department of Physics, University of Colorado, Boulder, Colorado 80309, USA

<sup>4</sup>Renewable and Sustainable Energy Institute, National Renewable Energy Laboratory and University of Colorado, Boulder, Colorado 80309, USA

<sup>5</sup>Department of Electromagnetic Engineering, Royal Institute of Technology, S-100 44 Stockholm, Sweden

 (Received 29 March 2019; revised manuscript received 4 June 2019; published 22 August 2019)

We present a controlled cascade of self-assemblies of colloidal droplets at a nematic liquid crystal–air interface into large-scale ordered structures. Changing the tilt of the droplet-induced elastic dipoles via its dependence on the nematic film thickness, we are able to control the dipole-dipole interaction and thus the self-assembling regime. For a progressively large tilt, droplets form anisotropic lattices, which then transform into arrays of repulsive chains, then to bands of half-period-shifted densely bound chains. These structures with chain order at the inner scale aggregate into different large-scale clusters that have a pronounced circular pattern and are stabilized by the many-body elastocapillary attraction.

DOI: [10.1103/PhysRevLett.123.087801](https://doi.org/10.1103/PhysRevLett.123.087801)

*Introduction.*—Elementary entities often tend to come together into fascinating arrangements at a larger scale. From this self-assembling (SA) we have learned that nature might provide us with structures that are beyond our imagination but, at the same time, if understood, can be controlled and used in applications. Moreover, as SA is a many-body phenomenon, it might reveal truly collective interactions that cannot manifest themselves in a few body system, but may play an unrecognized role in various biological and material processes.

A powerful source of SA is offered by nematic colloids [1–3]. The unique physics behind this lies in the analogy between the elastic interaction of colloidal particles via the nematic director and that of the electrostatic multipoles [4–7]. Elastic dipoles and quadrupoles form various ordered structures, ranging from chains to various colloidal crystals. While assembling a three-dimensional crystal requires dragging the particles by laser tweezers [8,9] or electrostatic charge stabilization to balance strong elastic forces [10], chains and two-dimensional (2D) crystals, both in a nematic liquid crystal (NLC) bulk [11–16] and at NLC surface [17–19], can result from SA. Because of the lower dimension of a surface, however, the colloidal structures at the NLC-air interface [17–19] are stable and can be manipulated easily. It was demonstrated in [19] that the transition between two different colloidal 2D lattices can be induced by tilting the elastic dipole induced by a particle captured at the nematic surface. This points to the possibility to use the tilt as a parameter to control SA at a NLC-air interface.

This Letter for the first time presents a controlled multiscale cascade of SAs of spherical droplets on a NLC-air interface. Depending on the above parameter, droplets form a hexagonal lattice, anisotropic lattice, or straight or kink chains; chains form large loose clusters or dense stretched coherent bunches that then form large dense roundish clusters. A many-body interaction is found to be essential: the large-scale structures are stabilized by the recently predicted collective capillary attraction [20,21]. A general elastic dipole, which is a second rank tensor rather than a vector, is a combination of the four basic dipolar types [22]. While so far only situations with a single uniaxial dipole have been encountered experimentally [9,11,13,17–19], we find that our spherical droplets essentially induce two different dipoles, uniaxial and banana or  $\gamma$  dipole, and a planar quadrupole [23] whose magnitudes depend on the director tilt  $\psi$  at the NLC-air interface. Our theory shows that the above sequence of structures corresponds to the progressively increasing tilt, which varies along with the thickness  $h$  of a hybrid NLC film.

*Experimental results.*—A layer of 65 wt % sulfuric acid with a thickness less than 1 mm was covered with a layer of a NLC E7 (HCCH, China) [24]. Its thickness  $h$  could be set in the range  $h \sim 0.9\text{--}10 \mu\text{m}$  by preparing different samples with a different amount of NLCs. The homeotropic anchoring at the air interface favors the director tilt (to the film normal)  $0^\circ$  and the degenerate planar anchoring at the acid interface favors tilt  $90^\circ$ . The actual boundary tilts however depend on  $h$ : the thinner the film the more the director tilt at the air surface deviates from  $0^\circ$ .

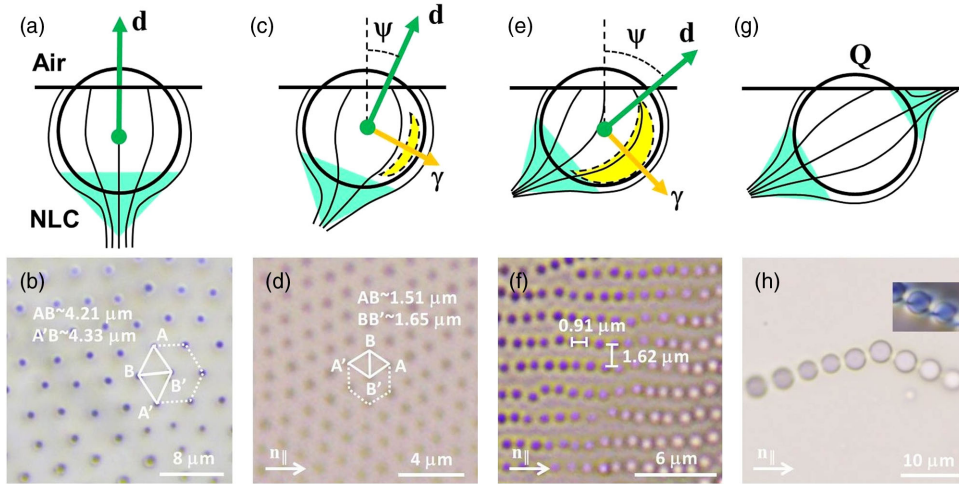


FIG. 1. The droplet-induced director patterns, which result in a uniaxial  $d$  dipole (green cone) and a  $\gamma$  dipole (yellow banana), depend on the director tilt  $\psi$  [(a), (c), and (e)] and lead to different structures [(b), (d), and (f)]; two opposite  $d$  dipoles (g) result in quadrupolar chains with kinks (h). The lattice anisotropy increases with  $\psi$ , which is larger for a larger ratio  $D/h$ : (b) ( $h, D \sim 10, 0.9 \mu\text{m}$ ), (d) ( $3, 0.6 \mu\text{m}$ ), (e) ( $2, 0.7 \mu\text{m}$ ), (h) ( $5, 3.9 \mu\text{m}$ ).

As NLCs contact the acid, copious droplets are generated. Some droplets move down to the bottom interface and enter the acid bulk, while others are trapped at the NLC-air interface. Then droplets grow through coalescence for minutes. As the droplets' diameter attains some stabilizing size  $D$ , the tangential anchoring at their surfaces induces director distortions sufficient to prevent further coalescence. Several factors determine droplet size. Among them the acid diffusion rate into NLCs is very important. It depends on the temperature gradient across the film, but it is difficult to control. Nevertheless, we have discovered that by decreasing  $h$  in a certain proportion, one is able to produce samples with roughly the same droplet size. Furthermore, droplet size and uniformity are also affected by the coalescence induced by NLC flowing, which should be prevented. This was achieved by making the surface of the sample flat (by reducing the contact angle of the acid solution on the glass) and spreading the NLC films all over the acid layer. The effective director tilt  $\psi$  at the droplet center is determined by  $D$  and director tilt at the air surface, which is set by the thickness  $h$ : the tilt is larger for larger diameter  $D$  and smaller  $h$ . The values of  $h$  were chosen in such a way that the tilt was progressively larger as  $h$  decreased in a certain range.

A droplet with the tangential anchoring trapped at the interface produces one point defect, boojum, near its lower pole or, for sufficiently large tilt  $\psi$ , also boojum near the upper pole, Fig. 1. In the first case, the droplet induces an elastic dipole, and the higher the boojum is shifted from the lower pole of the droplet, the greater the director tilt  $\psi$  at the droplet center. For small tilt (boojum close to the lower pole) droplets form large clusters that, at inner scale, are an anisotropic lattice close to hexagonal, Figs. 1(a)–1(d): distances between droplets in the two principal directions are only slightly different: 4.12 and 4.08  $\mu\text{m}$  [Fig. 1(b)],

1.51 and 1.65  $\mu\text{m}$  [Fig. 1(d)], and thermal motion is considerable. As the tilt increases, the anisotropy gets stronger until the lattice transforms into a system of parallel chains, Figs. 1(e) and 1(f), and then the second boojum appears, Fig. 1(g), and the chains have kinks, Fig. 1(h).

The further chains' SA also depends on  $\psi$ . For smaller  $\psi \sim 30^\circ$  ( $h \sim 0.9$ ,  $D \sim 0.3 \mu\text{m}$ ), chains form loose large clusters where they are separated by  $\rho \sim 1.64 \mu\text{m}$ , which is three times center-to-center distance  $a \sim 0.55 \mu\text{m}$  along the chain, Fig. 2. A mutual attraction of a few such chains has not been observed. For larger  $\psi \sim 50^\circ\text{--}60^\circ$  ( $h \sim 1.5 \mu\text{m}$ ,

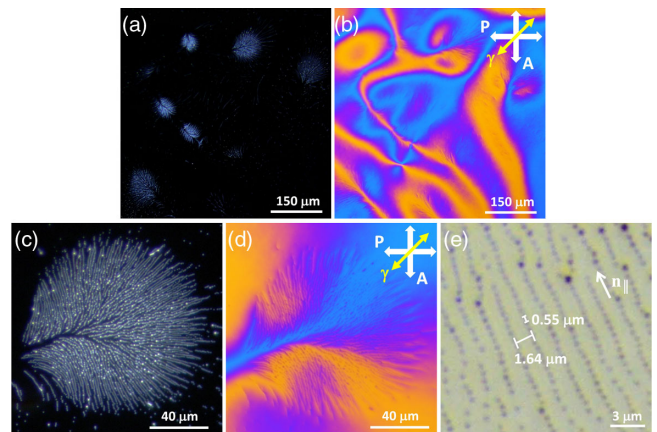


FIG. 2. (a) Dark field microscopic image of the droplet clusters for  $h \sim 0.9 \mu\text{m}$  and  $D \sim 0.3 \mu\text{m}$ . (b) Polarizing optical microscopic image of the same clusters with a phase retardation plate (530 nm  $\lambda$ -plate). (c) Zoomed-in image of one single cluster, which assumes circular form. (d) Polarizing optical microscopic image of the same cluster with a phase retardation plate (530 nm  $\lambda$ -plate). (e) Bright field image of the inner loose chain structure.  $\mathbf{P}$  and  $\mathbf{A}$  indicate the polarization directions of the polarizer and the analyzer;  $\gamma$  indicates the slow axis of the  $\lambda$ -plate.

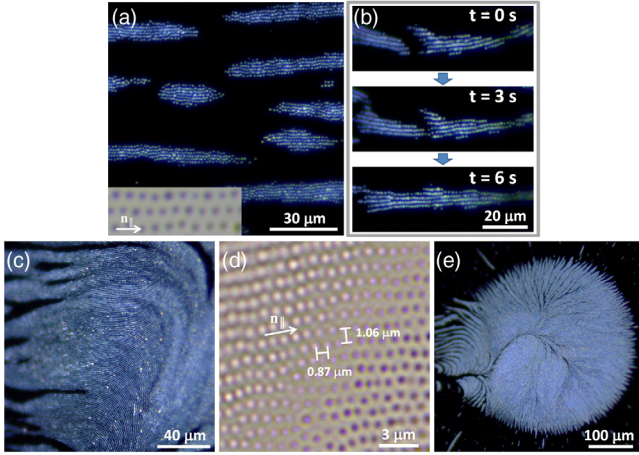


FIG. 3. (a) For  $h \sim 1.5$  and  $D \sim 0.7 \mu\text{m}$ , droplets first form bands with inner structure revealed in the inset. (b) Because of the long-range head-to-tail attraction, bands then form longer bands that aggregate into large dense clusters (c). (d) Zoomed-in image of dense clusters with coherent inner-scale structure where chains are displaced with respect to one another by one-half of the lattice spacing. (e) The final large-scale cluster formed tends to exhibit circular form.

$D \sim 0.7 \mu\text{m}$ ), chains attract one another first forming dense coherent bands, Fig. 3(a), where chains are shifted relative to their neighbors by half of the period  $a$  and the droplets are almost touching, inset in Fig. 3(a). While two such chains exhibit side-to-side attraction only at very short distances  $\sim a$ , band islands tend to form larger aggregates showing long-distance attraction head to tail and no visible attraction side to side, Fig. 3(b). In turn, the large aggregates assemble into a large dense clusters, Figs. 3(c)–3(e). At last, for sufficiently large tilt  $\psi > \psi_Q \sim 60^\circ$ , the second upper boojum appears signaling the presence of a quadrupole component, and the chains have kinks, Fig. 1(h). Similar chains were observed in a NLC bulk and attributed to the quadrupole-quadrupole interaction [14]. More effects related to quadrupolar chains will be reported elsewhere. In samples with some thickness variation, transitions between different droplet structures can be observed.

The largest scale superstructures can occupy surface area up to  $0.1 \text{ mm}^2$ . Their size is mainly determined by the number of droplets and is not necessarily associated with the size of the domains of the same average director orientation. For all the above inner scale structures, be it a lattice, or loose or dense coherent chains, they have two common patterns. First, the constituent chains are stretched along the in-plane director component  $\mathbf{n}_{\parallel}$ , which undergoes spontaneous turns peculiar for azimuthally degenerated hybrid films [25]. The director orientation can be determined through polarizing optical microscopy imaging with a phase retardation plate ( $530 \text{ nm } \lambda$ -plate), e.g., Figs. 2(b) and 2(d). Second, there is a well-observed tendency for the large clusters to assume an overall circular form, Figs. 2(b)

and 3(e), indicating an existence of some centripetal force. Below we show that this force is a strong many-body elastocapillary effect that stabilizes clusters even as the droplets in lattice and loose clusters repel one another elastically.

*Theory.*—Each droplet induces certain elastic multipoles. First we note that the tilted dipole has two essential components, the standard uniaxial  $d$  dipole and negative  $\gamma$  or banana dipole [22,26], which can be conventionally depicted by the mutually perpendicular arrows [27], Fig. 1. Let  $\mathbf{n}$  be the nematic director extrapolated to the droplet center and  $\psi$  its tilt to the film normal. Figure 1 shows that both dipoles depend on  $\psi$ : the  $d$  dipole weakens and  $\gamma$  dipole strengthens as  $\psi$  increases. As a simple model we set  $d = d_0 \cos \psi$ ,  $\gamma = \gamma_0 \sin \psi$ . Let  $K$  be the elastic constant and  $\theta$  the angle between the separation vector  $\mathbf{r}$  and  $\mathbf{n}$ . Then the  $dd$ ,  $\gamma\gamma$ , and  $d\gamma$  interaction potentials are [22]

$$\begin{aligned} U_{dd} &= \frac{12\pi K}{r^3} d_0^2 \cos^2 \psi (1 - 3\cos^2 \theta), \\ U_{\gamma\gamma} &= -\frac{12\pi K}{r^3} \gamma_0^2 \sin^2 \psi (1 - 3\cos^2 \theta), \\ U_{\gamma d} &= \frac{9\pi K}{r^3} \gamma_0 d_0 \sin 2\psi \sin 2\theta \cos \phi, \end{aligned} \quad (1)$$

where  $\phi$  is the azimuthal angle defined in [22] (Supplemental Material). Consider two droplets at the NLC-air interface at a distance  $r$ , one at the center of a chain stretched along  $\mathbf{n}_{\parallel}$  and another one at distance  $\rho = r \sin \varphi$  from the chain, Fig. 4(a). The angles  $\theta$  and  $\phi$  can be expressed in terms of  $\varphi$  and  $\psi$  (Supplemental Material):  $\cos \theta = \sin \psi \cos \varphi$ ,  $\tan \phi = \sin \varphi / \cos \psi \cos \varphi$ . All the elastic dipolar effects described below are found by making use of these formulas in the total potential  $U = U_{dd} + U_{\gamma\gamma} + 2U_{\gamma d}$ . We found that  $\gamma_0/d_0 = -0.3$  is plausible and arrived at the following picture.

Droplets cannot form chains if  $\psi$  is too small. Nevertheless, they locate along the in-plane director line  $\mathbf{n}_{\parallel}$ ,  $\varphi = 0$ , as then their interaction has lower energy (repulsion is weaker). Hence interparticle distance along  $\mathbf{n}_{\parallel}$  is shorter than that in other directions, which is seen in the anisotropic lattices, Figs. 1(b) and 1(d). For sufficient tilt  $\psi > \psi_c \sim 30^\circ$ ,  $U$  becomes negative signaling an attraction and particles form chains.

Figure 4 demonstrates the general physical picture. For small droplet-chain distance  $\rho = 1.2$  (all distances are in units  $a \gtrsim D$ ), the interaction  $U_{d-c}(\delta)$  of a chain with  $N = 41$  droplets with a single droplet is always minimum as its shift  $\delta$  from the chain center is half-integer, Fig. 4(b). For  $\psi = 48^\circ$  even these minima are positive meaning repulsion; for  $\psi = \psi_{cc} = 50.3^\circ$ , attraction occurs for half-integer  $\delta$ ; and for  $\psi = 55^\circ$ , attraction occurs for any  $\delta$ . It is seen that a droplet is strongly attracted to the chain's end from outside for any  $\delta$ , which drives chain growth. Figure 4(c) shows that even for  $\psi = 55^\circ$  the attraction range is just a few droplet

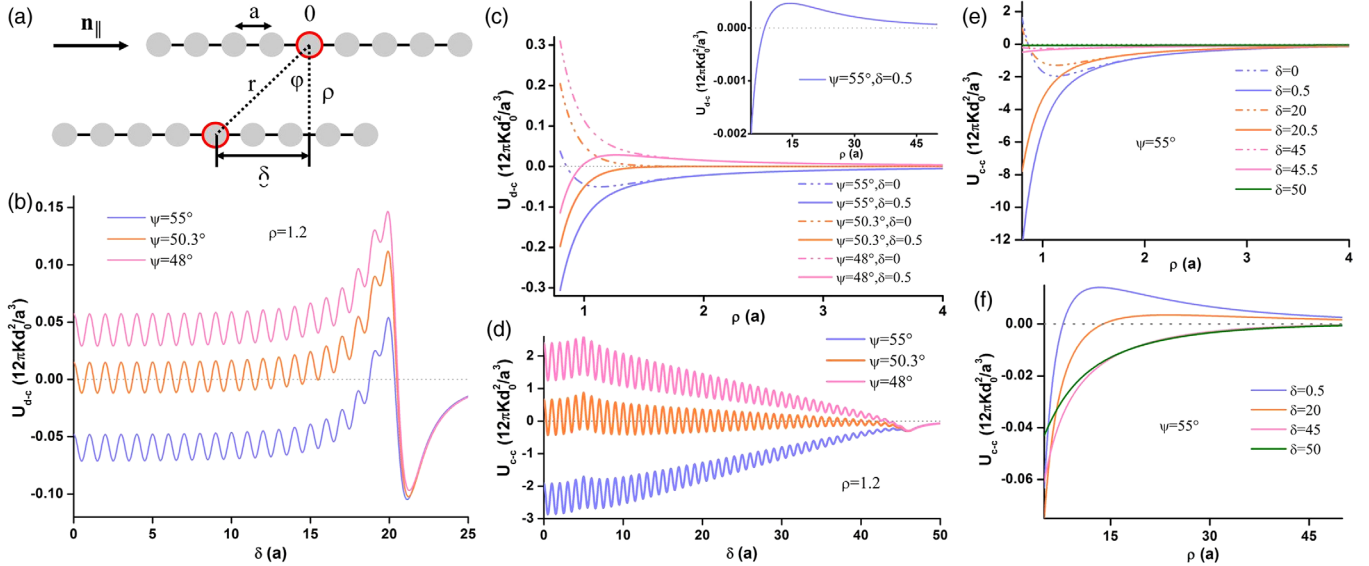


FIG. 4. (a) Schematic of two chains of droplets (all lengths are in units  $a$ ). (b) The interaction energy  $U_{d-c}(\delta)$  of a droplet with a chain with  $N = 41$  for  $\rho = 1.2$  and different  $\psi$ ; (c)  $U_{d-c}(\rho)$  for different  $\psi$  and  $\delta$ . (d) The interaction energy  $U_{d-c}(\delta)$  of two chains with  $N = 41$ ,  $N' = 51$  for  $\rho = 1.2$ ; [(e) and (f)]  $U_{c-c}(\rho)$  for  $\psi = 55^\circ$  and different  $\delta$ .

diameters, whereas at larger distances chains repel droplets, inset of Fig. 4(c).

The chain-chain interaction  $U_{c-c}$  is obtained by summation of the above  $U_{d-c}$  over different shifts. The side-to-side interaction of two chains (small center-to-center shift  $\delta$ , high chains' overlapping) with  $N = 41$  and  $N' = 51$  droplets is minimum for half-integer  $\delta$ ; for  $\psi \sim \psi_{cc} \approx 50^\circ$ , attraction is only for half-integer  $\delta$ , and for  $\psi = 55^\circ$ , attraction is for any  $\delta$ , Fig. 4(d). This side-to-side attraction is short ranged, Figs. 4(e) and 4(f). However, in the geometry close to head to tail (large shift  $\delta > N/2 + N'/2$ ), chains are attracted at appreciable  $\rho$  and any  $\delta$ , Fig. 4(f). As the head-to-tail attraction is roughly  $\propto NN'$ , band islands consisting of several chains can move toward one another, connecting into one longer cluster. This explains the repulsion of chains in loose clusters, coherent short-distance attraction of chains in dense clusters, and why two band clusters are not attracted side to side, but can move head to tail as to close the gap and stretch along a common in-plane director line. We stress that having the  $\gamma$  dipole is essential: without it the chain-chain attraction would require a large  $\psi > 75^\circ$ . However, for even smaller  $\psi$  we observe the second boojums and quadrupolar chains with kinks.

An attraction that stabilizes elastically repulsive loose clusters and lattices is a many-body elastocapillary effect. As a droplet is not fully submerged in the NLC, the elastic pressure, equal to the distortion free energy density at the NLC-droplet interface [31], produces a net upward force  $f$  proportional to the surface area  $S_{\text{cup}}$  within the contact line:  $f \sim (K/2)(S_{\text{cup}}/R^2) = \alpha K$ , where  $\alpha \sim 0.5$  is a numerical constant and  $R = D/2$  is the droplet's radius. This force induces a pairwise attraction with the potential  $U_2(r) = (f^2/2\pi\sigma)\ln(r/2\lambda)$  where  $\sigma = 4 \times 10^{-2} \text{ J m}^{-2}$  is

the surface tension at the NLC-air interface and  $\lambda \sim 10^3 \mu\text{m}$  the capillary length [32,33]. For the smallest related distance  $\sim 3a = 1.6 \mu\text{m}$  and  $K \sim 10^{-11} \text{ N}$ ,  $U_2 \sim -0.2kT$ . At the same time, in a lattice of vertical dipoles ( $\psi = 0$ ,  $d \sim R^2$ ) the pair repulsion energy at this distance is a few orders of magnitude larger,  $U_{dd} \sim 10^2 kT$ , and the pairwise force cannot stabilize the elastic repulsion. However, in a system of  $N$  particles with the long-range logarithmic  $U_2$ , the interaction is a collective effect: the interaction of a particle with the closest neighbors is weaker than that with far particles, and the total energy is proportional to  $N^2$  rather than to  $N$  so that the interparticle force  $\propto N$ . For spherical particles on a liquid-gas interface the collective effect was derived in [20,21]. In a circular cluster of  $N$  particles with the radius  $R_N < \lambda$ , the attraction energy per particle is  $U_N \simeq -(f^2/\pi\sigma)N$  [21]. Obviously, for sufficiently large  $N \gtrsim 100$ , one has  $U_{dd} \sim -U_N$  so that this attraction can stabilize the elastic repulsion. This is in line with our observation that loose clusters with more than about 20 droplets become more and more stable with respect to the thermal motion and droplet loss. Moreover, we can estimate the upthrust  $f$  from the condition that adding one particle to a small cluster of size  $N$  lowers its energy by the thermal energy  $kT$  [21]. For our dipolar repulsive force  $\propto r^{-4}$  and  $N = 20$  it gives  $f \sim \sqrt{2\sigma kT/N} \approx 0.3 \times 10^{-11} \text{ N}$  in accord with the above value  $f \sim 0.5 \text{ K}$ . The collective attraction at the scale of a whole cluster is centripetal and it is this force that induces the circular patterns observed in the large-scale superstructures.

*Conclusion.*—Nematic colloids are famous for the great versatility of ordered structures and there is a need to control their formation [34–36]. Reduction to two

dimensions makes this easier. Recent developments in the study of colloidal particles at a NLC-air interface have pointed out that tilting the trapped elastic dipoles is a possible means to switch between two different structures [19]. We have developed the first experimental multistep realization of this idea by designing a tilt-controlled cascade of switching between different SA regimes. The method proved to be fruitful: we have found novel ordered structures in the sequence that shed light on their causality. The collective attraction in clusters of spherical colloidal particles was unambiguously confirmed and the nature of the elastic upthrust was clarified. At last, our findings also demonstrate a highly nontrivial fact that the elastic multipole approximation is a reliable tool to study 2D nematic colloids.

This work was supported by the National Natural Science Foundation of China (Grants No. 91833303, No 61850410525, and No. 11621101), and the National Key Research and Development Program of China (Grant No. 2017YFA0205700). V. M. P.'s work was supported by VC 202 from NAS of Ukraine.

N. W. and J. S. E. contributed equally to this work.

\*Corresponding author.

sailing@kth.se

<sup>†</sup>victorpergam@yahoo.com

<sup>‡</sup>ivan.smalyukh@colorado.edu

<sup>§</sup>juliane@colorado.edu

- [1] P. Poulin, H. Stark, T. C. Lubensky, and D. A. Weitz, *Science* **275**, 1770 (1997).
- [2] I. Muševič, *Liquid Crystal Colloids* (Springer, Berlin, 2017).
- [3] I. I. Smalyukh, *Annu. Rev. Condens. Matter Phys.* **9**, 207 (2018).
- [4] S. Ramaswamy, R. Nityananda, V. A. Gaghunathan, and J. Prost, *Mol. Cryst. Liq. Cryst.* **288**, 175 (1996).
- [5] T. C. Lubensky, D. Pettey, N. Currier, and H. Stark, *Phys. Rev. E* **57**, 610 (1998).
- [6] B. I. Lev and P. M. Tomchuk, *Phys. Rev. E* **59**, 591 (1999).
- [7] V. M. Pergamenschchik, *J. Mol. Liq.* **267**, 337 (2018).
- [8] I. Muševič, M. Škarabot, D. Babič, N. Osterman, I. Poberaj, V. Nazarenko, and A. Nych, *Phys. Rev. Lett.* **93**, 187801 (2004).
- [9] A. Nych, U. Ognysta, M. Škarabot, M. Ravnik, and S. Žumer, *Nat. Commun.* **4**, 1489 (2013).
- [10] H. Mundoor, B. Senyuk, and I. I. Smalyukh, *Science* **352**, 69 (2016).
- [11] J.-C. Loudet, P. Borois, and P. Poulin, *Nature (London)* **407**, 611 (2000).
- [12] I. I. Smalyukh, O. D. Lavrentovich, A. N. Kuzmin, A. V. Kachynski, and P. N. Prasad, *Phys. Rev. Lett.* **95**, 157801 (2005).
- [13] M. Škarabot, M. Ravnik, S. Žumer, U. Tkalec, I. Poberaj, D. Babič, N. Osterman, and I. Muševič, *Phys. Rev. E* **76**, 051406 (2007).
- [14] M. Škarabot, M. Ravnik, S. Žumer, U. Tkalec, I. Poberaj, D. Babič, N. Osterman, and I. Muševič, *Phys. Rev. E* **77**, 031705 (2008).
- [15] U. Ognysta, A. Nych, V. Nazarenko, I. Muševič, M. Škarabot, M. Ravnik, S. Žumer, I. Poberaj, and D. Babič, *Phys. Rev. Lett.* **100**, 217803 (2008).
- [16] B. Senyuk, Q. Liu, S. He, R. D. Kamien, R. B. Kusner, T. C. Lubensky, and I. I. Smalyukh, *Nature (London)* **493**, 200 (2013).
- [17] V. G. Nazarenko, A. B. Nych, and B. I. Lev, *Phys. Rev. Lett.* **87**, 075504 (2001).
- [18] I. I. Smalyukh, S. Chernyshuk, B. I. Lev, A. B. Nych, U. Ognysta, V. G. Nazarenko, and O. D. Lavrentovich, *Phys. Rev. Lett.* **93**, 117801 (2004).
- [19] A. B. Nych, U. M. Ognysta, V. M. Pergamenschchik, B. I. Lev, V. G. Nazarenko, I. Muševič, M. Škarabot, and O. D. Lavrentovich, *Phys. Rev. Lett.* **98**, 057801 (2007).
- [20] V. M. Pergamenschchik, *Phys. Rev. E* **79**, 011407 (2009).
- [21] V. M. Pergamenschchik, *Phys. Rev. E* **85**, 021403 (2012).
- [22] V. M. Pergamenschchik and V. A. Uzunova, *Phys. Rev. E* **83**, 021701 (2011).
- [23] V. M. Pergamenschchik and V. A. Uzunova, *Condens. Matter Phys.* **13**, 33602 (2010).
- [24] Compared with the system of 5CB and glycerol, E7 and sulphuric acid solution can easily produce smaller colloids and a larger number of colloids in thinner nematic layers, which is necessary for the study of the self-assembly with large director tilt at the interface and the collective behavior of the droplets. No chiral effects are observed in the system of E7 and sulphuric acid solution.
- [25] O. D. Lavrentovich and V. M. Pergamenschchik, *Int. J. Mod. Phys. B* **09**, 2389 (1995).
- [26] The classification of elastic dipoles [22] shows that the pair  $d$ ,  $\gamma$  must be accompanied by a biaxial component  $\Delta$ . For simplicity justified by the outcome of our model, we assume  $\Delta$  to be small.
- [27] See Supplemental Material at <http://link.aps.org/supplemental/10.1103/PhysRevLett.123.087801> for the conventional and elastic-charge-related ways to depict elastic dipoles, which includes Refs. [5,22,28–30].
- [28] C. P. Lapointe, T. G. Mason, and I. I. Smalyukh, *Science* **326**, 1083 (2009).
- [29] V. M. Pergamenschchik and V. O. Uzunova, *Phys. Rev. E* **76**, 011707 (2007).
- [30] V. M. Pergamenschchik and V. A. Uzunova, *Eur. Phys. J. E* **23**, 161 (2007).
- [31] P. de Gennes and J. Prost, *The Physics of Liquid Crystals* (Clarendon, Oxford, 1993).
- [32] M. M. Nicolson, *Math. Proc. Cambridge Philos. Soc.* **45**, 288 (1949).
- [33] D. Y. C. Chan, J. D. Henry, and L. R. White, *J. Colloid Interface Sci.* **79**, 410 (1981).
- [34] O. P. Pishnyak, S. V. Shiyankovskii, and O. D. Lavrentovich, *Phys. Rev. Lett.* **106**, 047801 (2011).
- [35] N. M. Silvestre, Q. Liu, B. Senyuk, I. I. Smalyukh, and M. Tasinkevych, *Phys. Rev. Lett.* **112**, 225501 (2014).
- [36] S. Park, Q. Liu, and I. I. Smalyukh, *Phys. Rev. Lett.* **117**, 277801 (2016).